Chapter 27
The Formation of Protostars

The Jeans criterion derived in the foregoing section follows from a first-order perturbation theory and gives conditions under which perturbations of an equilibrium stage will grow exponentially. But the linear theory does not give information, for instance, about the fully developed collapse, to say nothing about the final product. For this, one has to follow the perturbation into the non-linear regime. We first begin with some very simple cases, assuming always spherical symmetry for the collapsing cloud.

27.1 Free-Fall Collapse of a Homogeneous Sphere

If, according to the Jeans criterion, a gaseous mass has become unstable and the collapse has started, gravity increases relatively more than the pressure gradient. The collapse is more and more governed by gravity alone, which is easily seen from the following arguments. For spherical symmetry, the gravitational acceleration is of the order GM/R^2, where M and R are the mass and radius of the cloud. On the other hand, an estimate of the acceleration due to the pressure gradient is

$$\left|\frac{1}{\varrho}\,\frac{\partial P}{\partial r}\right| \approx \frac{P}{\varrho R} \approx \frac{\Re}{\mu}\frac{T}{R}. \tag{27.1}$$

The ratio of gravitational force to pressure gradient is therefore $\sim M/(RT)$, which during isothermal collapse increases as $1/R$. Consequently we here neglect the gas pressure.

The free collapse of a homogeneous sphere can be treated analytically. At a distance r from the centre the gravitational acceleration is Gm/r^2, where m is the mass within the sphere of radius r. If the pressure can be neglected, the sphere collapses in free fall, according to the equation of motion

$$\ddot{r} = -\frac{Gm}{r^2}, \tag{27.2}$$

R. Kippenhahn et al., *Stellar Structure and Evolution*, Astronomy and Astrophysics Library, DOI 10.1007/978-3-642-30304-3_27, © Springer-Verlag Berlin Heidelberg 2012

where the dots indicate the time derivatives of the radius $r(m,t)$. We now replace m by $4\pi\,\varrho_0 r_0^3/3$, where the subscript zero indicates the values at the beginning of the collapse, by assumption $\varrho_0 = \text{constant}$. Multiplication of (27.2) by $\dot{r}$ and integration gives

$$\frac{1}{2}\dot{r}^2 = \frac{4\pi r_0^3}{3r} G\varrho_0 + \text{constant}. \tag{27.3}$$

Choosing the integration constant so that $\dot{r} = 0$ at the beginning, when $r = r_0$, we get

$$\frac{\dot{r}}{r_0} = \pm\left[\frac{8\pi G}{3}\varrho_0\left(\frac{r_0}{r} - 1\right)\right]^{1/2}. \tag{27.4}$$

In order to obtain only real values of r, it must always be less than r_0, which means that only the minus sign on the right of (27.4) gives relevant solutions.

For the solution of (27.4) we introduce a new variable ζ, defined by

$$\cos^2\zeta = \frac{r}{r_0}. \tag{27.5}$$

Therefore

$$\frac{\dot{r}}{r_0} = -2\,\dot{\zeta}\cos\zeta\sin\zeta, \quad \frac{r_0}{r} - 1 = \frac{\sin^2\zeta}{\cos^2\zeta}, \tag{27.6}$$

and (27.4) gives

$$2\,\dot{\zeta}\cos^2\zeta = \left(\frac{8\pi G\varrho_0}{3}\right)^{1/2}. \tag{27.7}$$

With the identity

$$2\,\dot{\zeta}\cos^2\zeta = \frac{d}{dt}\left(\zeta + \frac{1}{2}\sin 2\zeta\right), \tag{27.8}$$

which is easily verified, we can write instead of (27.7) that

$$\zeta + \frac{1}{2}\sin 2\zeta = \left(\frac{8\pi G\varrho_0}{3}\right)^{1/2} t, \tag{27.9}$$

where the integration constant is chosen such that the beginning of the collapse (when $r = r_0$ or $\zeta = 0$) coincides with $t = 0$. It should be noted that r_0 no longer explicitly appears in the solution (27.9) and that $\varrho_0 = \text{constant}$. Therefore the solution $\zeta(t)$ is the same for all mass shells. Then, according to (27.6), r/r_0 and also $\dot{r}/r_0$ at a given time t are the same for all mass shells. This means that the sphere undergoes a *homologous contraction*. Since $\dot{r}/r_0$ is independent of r_0, the relative density variation is independent of r_0, and the sphere, which was homogeneous at $t = 0$, remains homogeneous. The time it takes to reach the centre ($r = 0$ or $\zeta = \pi/2$) is the free-fall time

$$t_{\text{ff}} = \left(\frac{3\pi}{32G\varrho_0}\right)^{1/2}, \tag{27.10}$$

which follows from (27.9) and is the same for all mass shells. With $\varrho_0 = 4 \times 10^{-23}$ g/cm^3, corresponding to a slightly enhanced interstellar density, one obtains $t_{\text{ff}} \approx 10^7$years. For a typical protostellar clump as in Sect. 26.2, with $\varrho_0 = 4 \times 10^{-19}$ g/cm^3, (27.10) results in $t_{\text{ff}} \approx 2 \times 10^5$ years. It should be noted that expression (27.10) is very similar to the free-fall time τ_{ff} for a star we estimated in (2.17), if there g is replaced by $GM/R^2 = 4\pi G\varrho_0 R/3$.

Of course, before the centre is reached the pressure will become relevant as the gas becomes opaque and T increases. Then the free-fall approximation has to be abandoned, and finally the collapse will be stopped.

27.2 Collapse onto a Condensed Object

As the collapsing cloud becomes opaque the heating will first start in the central parts, since radiation can escape more easily from gas near the surface. Therefore the collapse will be stopped first in the central region. In order to see what then happens we consider a core which has already reached hydrostatic equilibrium, surrounded by a still-free-falling cloud. We emphasize that usually matter carries angular momentum, which is conserved, with the result that matter is first accumulated in an accretion disc around the central object, from where it finally flows onto the accreting body. This fact is ignored here.

Now let M be the mass of the core. For the sake of simplicity we neglect the self-gravity of the free-falling matter. The simplest case is that for the steady state. This would mean that the core is surrounded by an infinite reservoir of matter from which a steady flow rains down. Then the mass flow with absolute radial velocity v,

$$\dot{M} = 4\pi r^2 \varrho v, \tag{27.11}$$

must be constant in space and time. Differentiation of (27.11) with respect to r gives the continuity equation

$$\frac{2}{r} + \frac{1}{\varrho}\frac{d\varrho}{dr} + \frac{1}{v}\frac{dv}{dr} = 0. \tag{27.12}$$

If for v we take the free-fall velocity $v = v_{\text{ff}} = [GM/(2r)]^{1/2}$ and assume $M \approx$ constant, we find

$$\frac{1}{\varrho}\frac{d\varrho}{dr} = -\frac{3}{2r}, \tag{27.13}$$

or

$$\varrho(r) = \frac{\text{constant}}{r^{3/2}}. \tag{27.14}$$

If R is the radius of the core, then at impact the free-falling matter has the velocity $v_{\text{ff}}(R) = [GM/(2R)]^{1/2}$.

The matter falling onto the core is stopped at its surface. The kinetic energy is then transformed into heat, part of which is used to heat up the core, the rest being radiated away. If we ignore the heating of the core, the radiation losses are

$$L_{\rm accr} = \frac{1}{2} v_{\rm ff}^2(R)\dot{M} = \frac{1}{4}\frac{GM}{R}\dot{M}. \tag{27.15}$$

$L_{\rm accr}$ is called the *accretion luminosity*. Since for the steady-state solution we have assumed constant M in the expression for $v_{\rm ff}$, (27.15) is only valid if the accretion timescale

$$\tau_{\rm accr} := M/\dot{M} \tag{27.16}$$

is long compared to the free-fall time $t_{\rm ff}$.

27.3 A Collapse Calculation

The collapse of an unstable interstellar cloud can in principle be followed numerically. We will describe the first, meanwhile classical collapse calculations of a spherical, homogeneous cloud of one solar mass by Larson (1969). Although in the meantime three-dimensional hydrodynamical calculations have become possible, Larson's work is nicely illustrating basic effects and remains conceptionally very instructive. Modern one-dimensional calculations (e.g. Ogino et al. 1999) of collapsing Bonnor-Ebert spheres (see Sect. 26.2) give in fact results very similar to Larson's original models. The mass fractions of hydrogen, helium, and heavier elements were taken to be $X = 0.651$, $Y = 0.324$, and $Z = 0.025$, respectively. The boundary conditions assumed that the surface of the sphere remained fixed. The equations to be solved are the continuity equation

$$\frac{\partial m}{\partial t} + 4\pi r^2 v\varrho = 0 \tag{27.17}$$

(with the radial velocity v having positive values in outward direction), the equation of motion

$$\frac{\partial v}{\partial t} + v\frac{\partial v}{\partial r} + \frac{Gm}{r^2} + \frac{1}{\varrho}\frac{\partial P}{\partial r} = 0, \tag{27.18}$$

and the energy equation

$$\frac{\partial u}{\partial t} + P\frac{\partial}{\partial t}\left(\frac{1}{\varrho}\right) + v\left[\frac{\partial u}{\partial r} + P\frac{\partial}{\partial r}\left(\frac{1}{\varrho}\right)\right] + \frac{1}{4\pi\varrho r^2}\frac{\partial l}{\partial r} = 0, \tag{27.19}$$

where u is the internal energy per unit mass. Here the terms on the left (except for the last one) give the substantial derivative $du/dt + Pd(1/\varrho)/dt$ according to $d/dt = \partial/\partial t + v\partial/\partial r$. In addition we have the relation

$$\frac{\partial m}{\partial r} = 4\pi r^2 \varrho. \tag{27.20}$$

Finally we need an equation which describes the energy transport by radiation. Although the diffusion approximation is certainly not good in those parts of the cloud which are optically thin (see Chap. 5), the equation

$$l = -\frac{16\pi a c r^2}{3\kappa\varrho} T^3 \frac{\partial T}{\partial r} \tag{27.21}$$

was used, which is identical with our equation (5.11). The errors introduced do not change the qualitative (and maybe even the quantitative) results too much.

For the absorption properties of a gas at extremely low temperatures, other effects than those due to atomic absorption and scattering discussed in Chap. 17 have to be considered. As long as they exist, dust grains are the dominant source of opacity. With increasing temperature (above 1,000 K) the dust particles evaporate. Then the collapsing material becomes more transparent, the opacity being dominated by molecules (Sect. 17.8).

With (27.17)–(27.21), one has five equations for the five unknown variables $m(r, t)$, $v(r, t)$, $P(r, t)$, $T(r, t)$, and $l(r, t)$, while ϱ, κ, and u are given material functions of, say, P and T. The equation of state is assumed to be that of an ideal gas (including effects of dissociation and ionization). The numerical solution now has to be determined with one of the methods described in Sect. 12.3. The outer boundary condition at $r = R$ in these calculations is $v(R, t) = 0$. Since the equations show a singularity at the centre, one has to demand as inner boundary condition that the solutions remain regular there. The initial conditions are $v(r, 0) = 0$, while $P(r, 0)$ and $T(r, 0)$ are constant, and therefore $l(r, 0) = 0$. The initial values were $T(r, 0) = 10\,\mathrm{K}$, $\varrho(r, 0) \approx 10^{-19}\,\mathrm{g/cm^3}$. It should be noted that then almost all hydrogen is in molecular form. These are exactly the conditions we used for the derivation of the typical Jeans mass for a realistic collapsing clump in Sect. 26.2.

In order to have instability at the beginning, the cloud of one solar mass must be sufficiently dense and therefore small. Instability was found numerically by Larson (1969) for $R < 0.46 GM\mu/(\Re T)$. The close resemblance to the critical radius (26.27) for *homologous* collapse should be noted. The calculations began with a slightly compressed cloud with $R = 1.63 \times 10^{17}\,\mathrm{cm}$. With the density $10^{-19}\,\mathrm{g\,cm^{-3}}$ the free-fall time is $6.6 \times 10^{12}\,\mathrm{s} \approx 210,000$ years, according to (27.10), where we already estimated such a value.

In the following we describe the different phases of the collapse.

27.4 The Optically Thin Phase and the Formation of a Hydrostatic Core

In the very first phase the whole collapsing cloud remains optically thin and therefore nearly isothermal with $T \approx 10\,\mathrm{K}$.

When the instability evolves into the non-linear regime the collapse becomes non-homologous, which is not surprising in view of the outer boundary condition. It holds the outer layers of the sphere at a fixed radius while the inner part is free to collapse. Indeed during collapse the density increases rapidly in the central part, while it remains practically constant in the outer regions. A small central concentration, once formed, will necessarily enhance itself. The free-fall time of a certain mass shell at distance r from the centre is of the order $[G\bar{\varrho}(r)]^{-1/2}$, where $\bar{\varrho}(r)$ is the mean density inside the sphere of radius r. If $\bar{\varrho}$ increases towards the centre, then the (local) free-fall time decreases in this direction. Therefore the inner shells fall faster than the outer ones, and the central density concentration becomes even more pronounced.

The calculations show that the density distribution–starting from $\varrho = \text{constant}$–approaches the form $\varrho \sim r^{-2}$ over gradually increasing parts of the cloud (see Fig. 27.1). It is not surprising that it does not follow (27.14), since there we have made assumptions (steady state, a free fall determined only by the gravity of a central object, ignoring gas pressure) which are not fulfilled here.

The density profiles in Fig. 27.1 can be described as follows. A smaller and smaller homogeneous mass collapses more and more rapidly, continuously leaving behind more matter in the inhomogeneously contracting envelope. There the timescale of collapse remains much larger because (1) the density is smaller and (2) pressure gradients brake the free fall.

The collapse of the homogeneous central part resembles a free fall as long as the matter can get rid of the released gravitational energy via radiation. The central region becomes opaque once a central density of $10^{-13}\,\mathrm{g\,cm^{-3}}$ is reached. Now the further increase of density in the centre causes an adiabatic increase of temperature. As a consequence the pressure there increases until the free fall is stopped.

This leads to the formation of a central core in hydrostatic equilibrium surrounded by a still-falling envelope. Immediately after the core has reached hydrostatic equilibrium, its mass and radius are $10^{31}\,\mathrm{g}$ and $6 \times 10^{13}\,\mathrm{cm}$, similar to the values estimated in Sect. 26.3 for the Jeans mass at the end of fragmentation, and the central values are $\varrho_\mathrm{c} = 2 \times 10^{-10}\,\mathrm{g\,cm^{-3}}$, $T_\mathrm{c} = 170\,\mathrm{K}$. The free-fall velocity at the surface of the core is 75 km/s. With increasing core mass and decreasing core radius, the velocity of the falling material exceeds the velocity of sound in the core surface regions. Therefore a spherical shock front is formed which separates the supersonic "rain" from the hydrostatic interior. In this shock front the falling matter comes to rest, releasing its kinetic energy. If all the energy released is radiated away (which is approximately the case), the luminosity of the accreting core is given by (27.15).

In certain respects the hydrostatic core resembles a star. But while the surface pressure is virtually zero for a star, here it has to balance the pressure exerted by the infalling material. If v_e and ϱ_e are the velocity relative to the shock front and the density of the falling gas just above it, respectively, and if P_i is the surface pressure, then conservation of momentum demands that

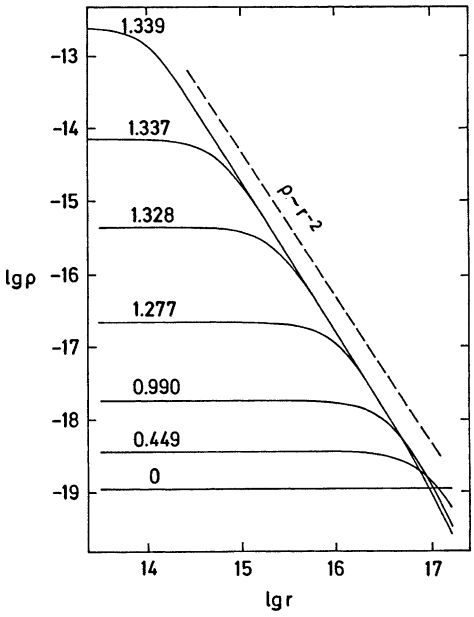

Fig. 27.1 The density ϱ (in $\mathrm{g\,cm^{-3}}$) against the distance from the centre r (in cm) in a collapsing cloud. The density distribution is shown by *solid lines* for different times (labels in 10^{13} s after the onset of the collapse). Regions with homologous changes remain homogeneous ($\partial\varrho/\partial r = 0$); regions in free fall approach a distribution with $\varrho \sim r^{-2}$ (i.e. a slope indicated by the *dashed line*) (After Larson 1969)

$$P_\mathrm{i} = \varrho_\mathrm{e} v_\mathrm{e}^2 = \varrho_\mathrm{e} \frac{GM}{2R}, \tag{27.22}$$

where M and R are the mass and radius of the core. This equation is a special case of the more general condition for shock fronts (see Landau and Lifshitz 1987, Vol. 6, p. 320) according to which the quantity $P + \varrho v^2$ must have the same values on both sides of the front. In (27.22) P is neglected outside the front and v inside.

Another difference between an accreting core and a real star is that the accretion energy is released in a thin surface layer, while in a star, the energy source is in the deep interior.

At first glance one would expect the whole core to be isothermal. But while matter is raining down on its surface the core is contracting. This has the consequence that L_accr as given by (27.15) increases for $\dot{M} \approx$ constant (since M grows and R decreases). Since during contraction gravitational energy is released in the deep interior of the core, there must be a finite temperature gradient in order to transport this energy outwards. The diameter of the accreting core in hydrostatic equilibrium is already comparable to the dimensions of the solar system (see Fig. 27.2).

27.5 Core Collapse

The accreting hydrostatic core heats up in its interior. We have to keep in mind that the gas consists mainly of hydrogen that at low temperatures is in molecular form as H_2. When the central temperature reaches about 2,000 K, the hydrogen

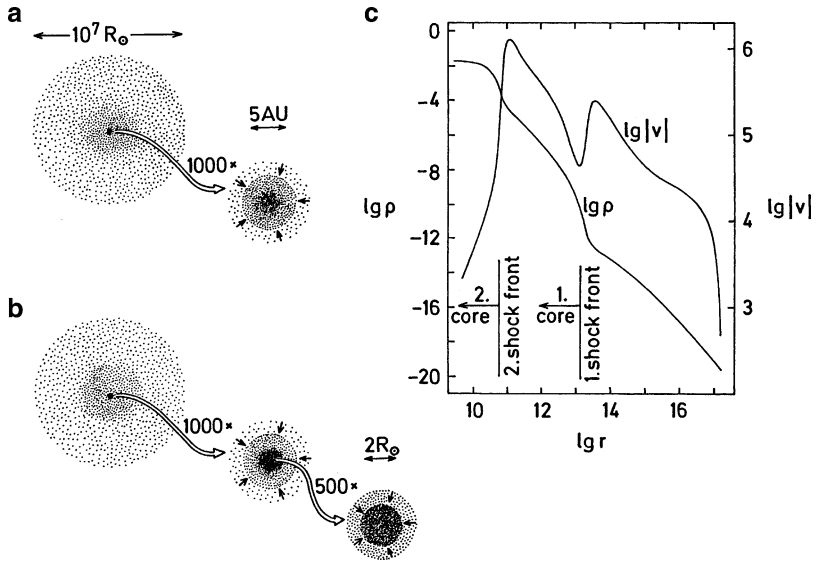

Fig. 27.2 The collapse of a gas cloud of $1M_\odot$. (**a**) After about 1.3×10^{13} s, the cloud has formed an optically thick core. The collapse is stopped there, and a shock front develops at the interface between the core, which is in hydrostatic equilibrium, and the still freely falling envelope. (**b**) When the core has become dynamically unstable owing to dissociation of H_2, a second collapse occurs within the core, forming a second shock front at much smaller r. (**c**) Schematic plot of the absolute value of the velocity v (in $\mathrm{cm\,s^{-1}}$) and the density ϱ (in $\mathrm{g\,cm^{-3}}$) against r (in cm), for a time shortly after the formation of a second core within the first one. The regions of the shock fronts are characterized by steep (positive) slopes in the velocity curve

molecules dissociate. The equilibrium between molecular and atomic hydrogen is governed by an equation similar to the Saha equation (see Sect. 14.1). Like ionization, dissociation influences the specific heat, since not all the energy injected into a gas goes into kinetic energy, a fraction being used to break up the molecules into atoms. This decreases γ_{ad}. For hydrogen molecules there are $f = 5$ degrees of freedom, three belonging to translation and two to rotation around two possible axes. Consequently $\gamma_{\mathrm{ad}} = (f + 2)/f = 7/5 = 1.40$. This is much closer to the critical value $4/3 = 1.33$ (see Sect. 25.3.2) than in the case of a monatomic gas ($\gamma_{\mathrm{ad}} = 5/3 = 1.667$). Only a slight reduction of γ_{ad} owing to dissociation therefore brings it below the critical value $4/3$. Then the hydrostatic equilibrium becomes dynamically unstable, and the core starts to collapse again.

In Larson's calculations this happened when the core has, compared to the initial values, twice the mass and half the radius. It collapses as long as the gas is partially dissociated. When almost all hydrogen in the central region is in atomic form, γ_{ad} increases above $4/3$ (approaching the value $5/3$ for a monatomic gas) and the collapsing core forms a dynamically stable subcore in its interior. This core, which is generally called *protostar* has an initial mass of $1.5 \times 10^{-3} M_\odot$ and an initial radius of $1.3 R_\odot$. Its central density is $2 \times 10^{-2}\,\mathrm{g\,cm^{-3}}$ and the central temperature is

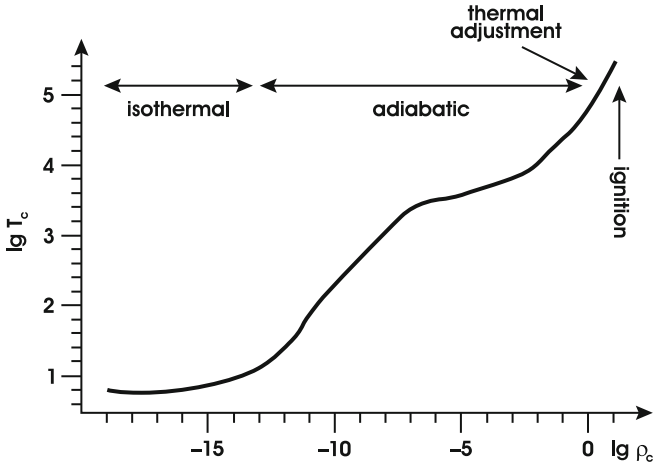

Fig. 27.3. The central evolution of a $1M_\odot$ cloud from the isothermal collapse to the ignition of nuclear burning. The central temperature T_c (in K) is plotted over the central density ϱ_c(in g cm^{-3}). (After Masunaga and Inutsuka 2000)

2×10^4 K. At the surface of this protostar there is another shock front. The situation is illustrated in Fig. 27.2b, c. As a consequence of the second collapse the density below the outer shock front decreases, and the outer shock finally disappears. More recent calculations by Masunaga et al. (1998) and Masunaga and Inutsuka (2000), which follow the collapse of a $1\ M_\odot$ clump through the whole sequence outlined above, confirm it to high degree. Their calculations include a better treatment of the radiative transport and can follow the collapse for a longer time due to a higher spatial resolution. The main difference with respect to Fig. 27.2c is that the velocities at the second shock front reach final values a factor of 10 higher than shown here, while the first shock front has already disappeared. The density profile is, however, very similar to that of Larson's original calculation.

The evolution of the centre of the $1M_\odot$ cloud, as it results from the radiation-hydrodynamical simulation by Masunaga and Inutsuka (2000), starting from the original Jeans instability, is given in Fig. 27.3. The curve starts on the left during the isothermal collapse. After the matter has become opaque, T rises adiabatically. The slope is at first close to 0.4 (corresponding to $\gamma_{ad} = 1.4$ for H_2), but then becomes considerably less owing to partial dissociation ($\gamma = 1.1$), and finally approaches $2/3$ (corresponding to $\gamma_{ad} = 5/3$ for a monatomic gas).

The central compression is adiabatic as long as the accretion timescale τ_{accr} of the core (or of the innermost core, if there are two) is short compared to its Kelvin–Helmholtz timescale τ_{KH}. But the more the envelope is depleted the more the accretion rate will diminish and consequently τ_{accr} will grow. When it exceeds τ_{KH} the core can adjust thermally and the evolution of the central region ceases to be adiabatic. Since then $\dot{M}$ has become very small, the protostar has practically

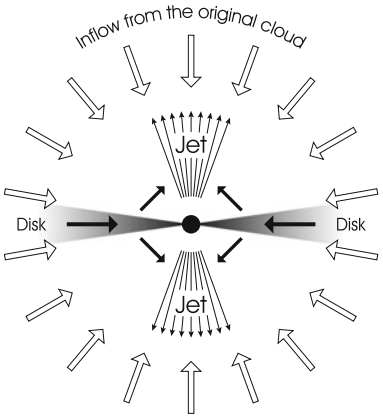

Fig. 27.4. Sketch of the mass flow within a collapsing protostellar sphere. From the original cloud, matter is accreted onto the protostar that sits at the centre of the figure. Because of angular momentum conservation, most of it accumulates in an accretion disc. Part of the matter finally falling onto the star is however ejected in a bipolar jet along the axis of rotation. The jet also may gain additional material directly from the disc due to heating of the inner disc (According to Zinnecker and Yorke 2007)

constant mass. We shall discuss its further evolution with constant M in the next section.

We repeat once more that these calculations were made without considering the fact that the angular momentum of the prestellar cloud leads to the formation of an accretion disc. Most of the matter falling onto the central protostar has first circled the star in this disc.

At the same time the protostar may start to lose mass due to stellar winds and bipolar outflows and jets. All this has already been revealed by observations. The interaction between cloud, protostar, and disc is complicated and also depends on the presence of magnetic fields. This phase has to be investigated by three-dimensional magnetohydrodynamical simulations (Banerjee and Pudritz 2007). The situation is illustrated in Fig. 27.4.

27.6 Evolution in the Hertzsprung–Russell Diagram

A plot of the evolution of a collapsing cloud in the Hertzsprung–Russell (HR) diagram has to be made with care. The radiation emitted by the core is absorbed in the falling envelope, particularly by dust grains, which heat up and reradiate in the infrared. One can assign an effective temperature to the protostellar models. Defining an effective radius R at the optical depth 2/3 one can derive an effective temperature $T_{\rm eff}$ from $L = 4\pi R^2 \sigma T_{\rm eff}^4$. Evolutionary tracks for initial masses of $1 M_\odot$ and $60 M_\odot$ are given in Fig. 27.5. Although the numerical

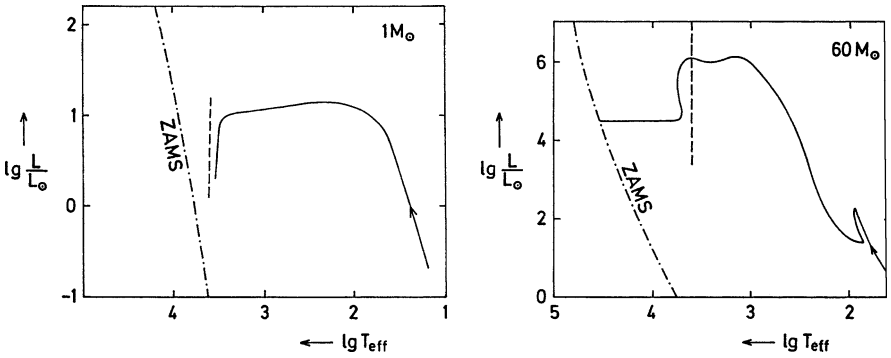

Fig. 27.5. Hertzsprung–Russell diagrams with evolutionary tracks for protostars of $1M_\odot$ and $60M_\odot$. The tracks start at the lower right, where the thermal radiation of the clouds is in the infrared, and they finally approach the zero-age main sequence (ZAMS, *dot-dashed*). In the case of $60M_\odot$, part of the mass of the envelope is blown away so that a star of only $17M_\odot$ settles down on the main sequence. The corresponding Hayashi lines are indicated by *broken lines* (After Appenzeller and Tscharnuter 1974, 1975a,b)

results shown in this figure are quite old, the newer calculations by Wuchterl and Tscharnuter (2003) have confirmed the overall picture very well. To an outside observer the collapsing cloud remains an infrared object as long as the envelope is opaque to visible radiation. The evolutionary track, therefore, starts extremely far to the right in this diagram. This, of course, is no contradiction to the statements about a forbidden region to the right of the Hayashi line (Chap. 24) since the falling envelope (including the "photosphere") is far from being in hydrostatic equilibrium. Even if we could see the already hydrostatic core, we would not observe a normal star, since its boundary conditions are still perturbed by infalling matter.

The thinning out of the envelope has several effects: the first is that it becomes more transparent, and the photosphere ($\tau = 2/3$) moves downwards until it has reached the surface of the hydrostatic core. With decreasing radius of the photosphere, $T_{\rm eff}$ must increase in order to radiate away the energy. In the whole first phase (through the maximum of L in the evolutionary tracks of Fig. 27.5) the luminosity is produced by accretion: $L = L_{\rm accr} \sim \dot{M}$. With decreasing $\dot{M}$, the luminosity L decreases until it is finally provided by contraction of the core.

It is generally found that for low-mass stars accretion onto the protostar stops well before central temperatures for hydrogen ignition is reached. For massive stars, however, accretion continues while central hydrogen burning has already set in. Therefore, when the newborn star finally separates from its surrounding cloud and becomes visible it has already consumed part of its hydrogen fuel and has evolved on the main sequence. Massive stars are therefore unlikely to be found on the ZAMS.

Another effect is the influence of accretion on the boundary conditions of the core. Strong accretion heats up the surface of the core so much that the core is nearly isothermal and the ram pressure $\varrho_{\rm e} v_{\rm e}^2$ is appreciable. With decreasing $\dot{M}$ the

boundary conditions become "normal". The core surface cools down, a temperature gradient is built up, and a convection zone develops downwards from the surface.

This convection may or may not penetrate down to the centre. If the object is fully convective, has "normal" boundary conditions, and is already visible, we must see it on the Hayashi line. In any case we have the transition from a protostar to a normal contracting star in hydrostatic, but not yet in thermal, equilibrium.

In this chapter we could only sketch the complicated and still not fully understood process of star formation. We concentrated on the evolution of individual contracting spheres that eventually become single stars, which is sometimes called the "classical picture" of star formation. In reality, stars form in clusters, which are the result of the many condensed regions of large molecular clouds, in which magnetic fields, turbulence, rotation, and gravity interact in complicated ways. We refer the reader to the reviews by Mac Low and Klessen (2004) and Zinnecker and Yorke (2007) for more details about this field.